ACS Photonics

Article

pubs.acs.org/journal/apchd5

High Temperature Nanoplasmonics: The Key Role of Nonlinear Effects

Alessandro Alabastri,* Andrea Toma, Mario Malerba, Francesco De Angelis, and Remo Proietti Zaccaria

Istituto Italiano di Tecnologia, via Morego 30, Genoa, 16163, Italy

ABSTRACT: In this work we show the effect of high temperature on the plasmonic properties of metallic nanorods. Within this context, the dielectric function of metal has been modified to keep into account both the electron−electron and electron−phonon temperature dependent scattering mechanisms. In fact, the mentioned damping processes are very sensible to temperature variation. It is found that the damping modifications due to temperature change substantially modify both the near and far field optical response of metallic nanorods. Furthermore, the response alteration can be very different depending on the rod aspect ratio, suggesting the need of accurate investigations when metallic nanostructures are to be employed within high-temperature environments or under high intensity irradiation. In this regard, by taking into account different nanorods aspect ratio and incident powers, we provide detailed calculations showing the error committed in evaluating absorption, scattering efficiencies, and near-field enhancement if the temperature dependence effect is neglected.

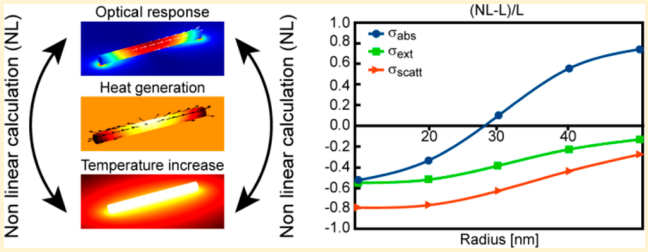

KEYWORDS: *thermo-plasmonics, nonlinear effects, photocatalysis, localized surface plasmon resonances, nanostructures*

Metallic nanostructures exhibit localized plasmon resonances (LPRs) that can be widely tuned by tailoring their shapes and background conditions.[1−12] This characteristic is very appealing inasmuch as the resonance tuning represents a fundamental aspect for sensing applications. In this regard, gold plays a major role owing to its plasmonic properties and its chemical resistance, which persist even at high temperatures where commercial sensors are still limited.[13] Even though both shape and geometry can be affected before reaching the melting temperature,[14] in the case of gold its stability has been preserved up to 800 °C[13,15] if nanoparticles are properly functionalized and placed, for instance, in a silica surrounding matrix. Interestingly, intrinsic plasmonic properties such as absorption and scattering efficiencies can be considerably modified when the environment temperature changes.[16,17] During the past decade, a lot of effort has been dedicated to the study of thermal effects due to energy dissipation by metallic nanostructures and the role played by temperature.[14,18−24] The main channel through which temperature influences the optical response of a metal is the damping factor, which enters its dielectric function. Recently, the authors proposed a nonlinear model to describe the permittivity of noble metals by taking into account the role of temperature while interacting with an electromagnetic field. The model was applied to gold spherical nanoparticles showing a sensible decrease of both scattering and absorption efficiency by temperature increase in good agreement with experimental measurements.[25] Here, we analyze gold nanorods[8,10] with different aspect ratios showing that, dissimilarly from spherical nanoparticles, a nonmonotone behavior is found with the temperature change. In particular, it is found that changing the radius of nanorods endowed with the same height can radically modify the trend of the absorption efficiency while tuning the background temperature. The results are compared with the outcomes from analogous geometrical systems where the standard permittivity description (no temperature-dependence) was instead assumed, finding striking differences. Therefore, the present study highlights the importance of a temperature-dependent damping term that can become quite crucial, especially when high temperature or high intensity radiation sources are considered, such as in photocatalysis[26,27] or for photon-enhanced thermionic emission applied to solar systems.[28] Indeed, the degrading of the optical parameters of gold, when exposed to high temperature, has led scientists to consider other plasmonic materials that can maintain their own stability in even more extreme conditions.[29−31]

Any metal dielectric function can be described by the Drude model combined with multiple Lorentzian oscillators that account for interband transitions:[32]

$$\varepsilon = 1 - \frac{\omega_p^2}{\omega[\omega - i\Gamma_{\text{Drude}}]} + \sum_{j=1}^{m} \frac{f_j \omega_p^2}{(\omega_j^2 - \omega^2) + i\omega\Gamma_j} \quad (1)$$

where Γ_{Drude} is the damping coefficient defined for bulk metals. In a more elaborated and realistic version[25] of eq 1, the Γ_{Drude} term is temperature T dependent ($\Gamma_{\text{Drude}} \rightarrow \Gamma(T)$) and it includes the electron−electron ($\Gamma_{\text{e-e}}$) and electron−phonon ($\Gamma_{\text{e-ph}}$) scattering mechanisms whose dependence on temperature was extensively studied.[33−41] Furthermore, we chose to describe the electron-surface ($\Gamma_{\text{e-surf}}$) scattering term as a

Received: September 4, 2014
Published: December 2, 2014

temperature independent quantity. More details about the modeling of the dielectric function and damping parameters can be found elsewhere.[25] However, it must be noticed that at optical or IR frequencies only electron−phonon scattering has a sensible dependence on temperature (linearly increasing).[25]

We consider isolated metallic nanorods in air with height h = 1 μm and radius R between 10 and 50 nm. The light source is a Gaussian beam defined by power P = 100 μW and beam waist w_0 = 1 μm impinging normal to the rods axis. The rationale is: under beam illumination dissipated energy is converted into heat, which increases the temperature of the nanorod. In turn, the temperature modifies the optical response of the system. This process leads to an iterative loop which eventually converges to a different solution than the result given by calculations with constant (no dependence on T) permittivity.

Within this framework, optical quantities such as absorption, scattering, electric field distribution, current density and in turn the temperature variation were calculated using two methods (see Figure 1a and 1b): standard linear (L) calculations by

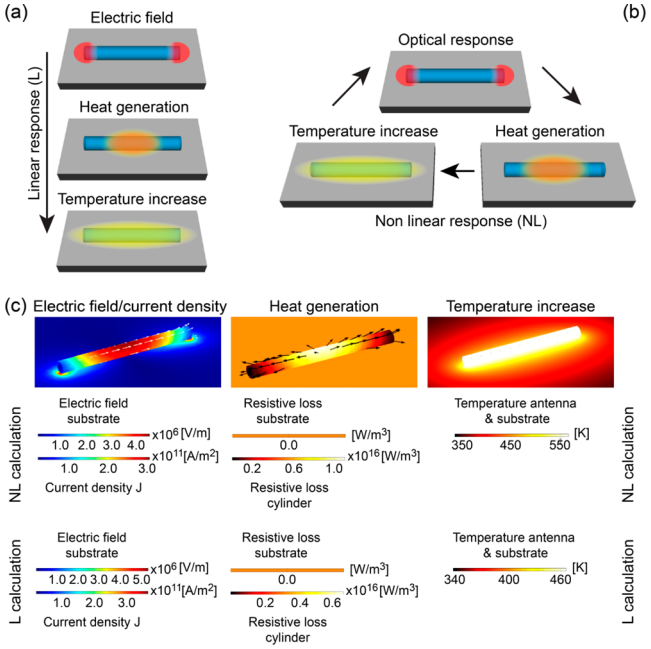

Figure 1. (a, b) Schematic comparison between the linear (L) and nonlinear (L) calculation paths. (c) Numerical calculations (Comsol Multiphysics) of a golden rod with 50 nm radius and 1 μm length interacting with an electromagnetic wave of power P = 100 μW and beam waist w_0 = 1 μm. Both the L and NL schemes are considered for comparison. The electric field distribution/current density, generated heat, and temperature distribution are shown (left to right). Color maps are shown for the NL case only.

means of a temperature independent damping term $\Gamma_L = \Gamma_{T\text{-amb}} + \Gamma_{e\text{-surf}}$ ($\Gamma_{T\text{-amb}}$ = 53 meV, corresponds to the room temperature damping value of gold,[32] while $\Gamma_{e\text{-surf}}$ keeps into account the electron−surface scattering and depends on the nanostructure geometry[25,42]), and nonlinear (NL) calculations, where the damping term is instead temperature dependent ($\Gamma_{NL} = \Gamma_{NL}(T) + \Gamma_{e\text{-surf}}$). The results were compared through the ratio (NL-L)/L (efficiency), calculated for each type of nanorod at its near-field resonant frequency. Figure 1c shows an example of L and NL numerical simulations where a golden rod 1 μm long with 50 nm radius was interacting with a Gaussian source of power 100 μW and beam waist 1 μm. The overlap of the near field distribution with the current density, the heat generation and the temperature distribution are shown in the figure. Interestingly, the temperature values predicted by the two models show a discrepancy of roughly 100 K.

Figure 2 demonstrates that the temperature dependent nonlinear model leads to very different results with respect to

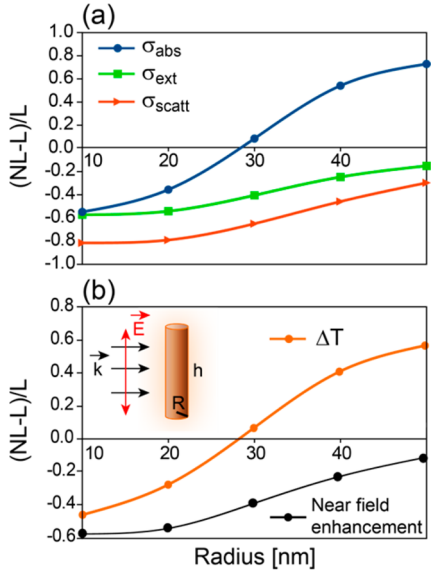

Figure 2. Ratio (NL-L)/L for (a) absorption efficiency (σ_{abs}), scattering efficiency (σ_{scatt}), and extinction efficiency (σ_{ext}); (b) temperature and near field enhancement calculated at 1 nm from the top of the metallic rod. The schematic of the isolated gold nanorods is shown in (b). The EM radiation is polarized along the rod main axis with power P = 100 μW and beam waist w_0 = 1 μm. The height of the rod is h = 1 μm. Different radii are considered: R = 10, 20, 30, 40, and 50 nm. The calculation was performed at the near field resonant wavelengths.

the linear model. Interestingly, for different radii, that is, at different resonant wavelengths, the mismatch among the solutions of the two models can be either positive or negative. Hence, it is not straightforward to predict the error which can be committed if temperature dependence is neglected. Rules of thumb or approximations might become difficult especially when high temperatures/high power sources are involved. In particular, we notice how the absorption efficiency σ_{abs} (Figure 2a) is under/overestimated by the L model for big/small radii. This effect explains the behavior of temperature increase shown in Figure 2b: since the absorption efficiency is related to Ohmic losses, it is connected to the temperature from a direct proportionality relation. In different words, the higher the absorption efficiency the higher the temperature, namely, a larger fraction of photons is converted into heat.

Regarding the other physical quantities shown in Figure 2, we observe how the NL model predicts lower values for scattering, near field enhancement and extinction than the L model for all the considered radii. These trends can have strong implications in different research fields, for example molecular nanophotonics, where nanoantennas are widely utilized,[43] or plasmonic photovoltaic, where the counterbalance between absorption and scattering plays a crucial role in the efficiency generation of e−h pairs.[44] In fact, a diminished scattering efficiency means less photons reirradiated from the nanostructures thus hindering detection measurements. A decreased near

dx.doi.org/10.1021/ph500326c | ACS Photonics 2015, 2, 115−120

field enhancement makes the system less efficient as near-field effects play an important role in a number of applications and, finally, a lower extinction translates into a reduced interaction between the structure and the incident electromagnetic field affecting the overall system performance.

In Figure 3 are presented the absorption and scattering efficiencies, calculated with the NL model, as a function of the

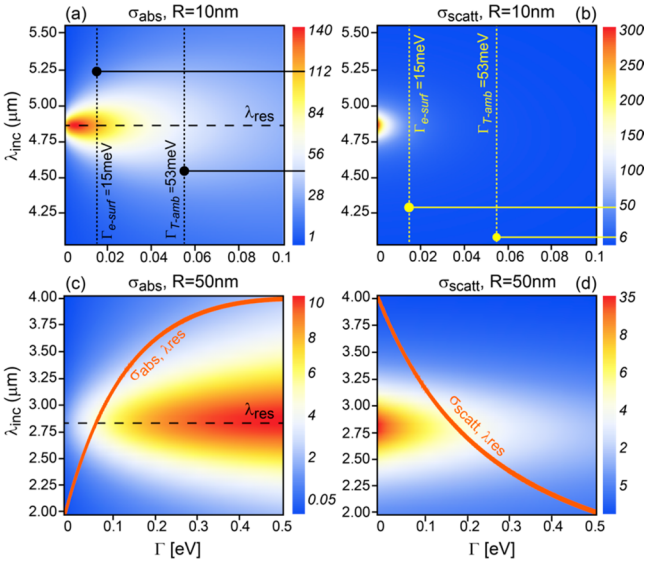

Figure 3. Nonlinear absorption and scattering efficiencies depending on incident wavelength and damping. (a) Absorption efficiency for 10 nm radius, (b) scattering efficiency for 10 nm radius, (c) absorption efficiency for 50 nm radius, (d) scattering efficiency for 50 nm radius. Rods height is kept constant at 1 μm. (a, c) also show the resonant wavelength λ_{res} for the 10 and 50 nm rod cases, respectively. Furthermore, (c) and (d) show the profile (orange curves) of the absorption and scattering efficiency calculated along the respective λ_{res} lines for the 50 nm rod configuration. Finally, the R = 10 nm case, illustrates the Γ values associated with the electron-surface scattering (15 meV) and to the ambient temperature (53 meV). In particular, the maximum values of σ_{abs} (σ_{scatt}) corresponding to $\Gamma_{e\text{-}surf}$ = 15 meV and to $\Gamma_{T\text{-}amb}$ = 53 meV are 112 (50) and 45 (6), respectively, as highlighted by the horizontal lines crossing the scale bars in (a) and (b).

incident wavelength λ_{inc} and the damping value Γ for the 10 and 50 nm radius cases. From the figure we observe a quite limited influence of the damping Γ on the resonant wavelength λ_{res} value, namely, the resonant wavelength is quite constant all across the observed Γ range. It depends only on the radius R. By taking into account the results of Figure 4a, namely the linear dependence between temperature T and damping Γ, we can move further by stating that the resonant wavelength λ_{res} does not depend on the temperature value.

Another important result shown in Figure 3a,c is the opposite behavior of σ_{abs} between the 10 and 50 nm radii cases, where the former shows a decrease of σ_{abs} by increasing Γ, vice versa the latter. These results can be explained by observing that the absorption efficiency is defined by the formula:

$$\sigma_{abs} = \frac{1}{2}\int_V \mathrm{Re}(\sigma)|E|^2(r)\mathrm{d}r/(cs_{rod}P_{IN}/a^2) \quad (2)$$

where σ is the electrical conductivity, cs_{rod} and a^2 are the cross section of the metallic rod and the overall area seen by the incoming radiation with power P_{IN}, respectively. In fact, from

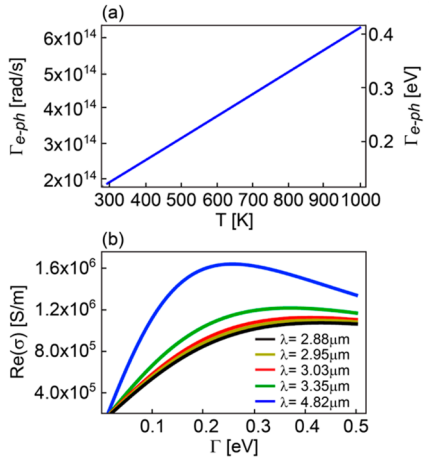

Figure 4. (a) Relation between the electron−phonon damping term $\Gamma_{e\text{-}ph}$ and the temperature T. Left and right vertical axis report the units in rad/s and eV, respectively. (b) Real part of the conductivity versus the total damping Γ. Different behaviors are found with respect to the near field resonant wavelengths, that is, rods aspect ratio.

eq 1 we see how the Re[$\sigma(\lambda,\Gamma)$] term plays a role in defining the absorption efficiency together with the electric field $E(\lambda,\Gamma,R)$. When the combination of the three independent variables (λ,Γ,R) is such to maximize both σ and E, the maximum σ_{abs} is reached. For example, the opposite behavior versus Γ shown by the 10 and 50 nm radii cases, can be explained in terms of Re[$\sigma(\lambda,\Gamma)$], as shown in Figure 4b: the λ = 4.82 μm (namely, R = 10 nm) plot illustrates a strong decrease of Re[σ] by increasing Γ, which supports the plot of Figure 3a. On the other hand, when the λ = 2.88 μm (namely, R = 50 nm) plot is considered, a monotone increase of Re[σ] is observed up to a plateau. This well describes Figure 3c. Importantly, analogous considerations can be done based on the behavior of the imaginary part of the permittivity, being ε and σ intimately related (Re(σ) = Im(ε)$\omega\varepsilon_0$; Im(σ) = (1 − Re(ε))$\omega\varepsilon_0$).

In Figure 3 is also reported the lowest Γ limit (i.e., $\Gamma_{e\text{-}surf}$), which is reached by reducing the temperature ($\lim_{T\to 0}\Gamma(T) = \Gamma_{e\text{-}surf}$). In particular, it is shown only for the R = 10 nm case ($\Gamma_{e\text{-}surf}$ = 15 meV); in fact, this value is neglectable for the R = 50 nm case. For completeness, also the total Γ value at room temperature is shown.

The concept of lowest Γ limit plays a crucial role for the optimization of the extinction efficiency $\sigma_{ext} = \sigma_{scatt} + \sigma_{abs}$. As shown by Figure 3, this condition tends to be reached by employing high-aspect ratio cylinders and low temperatures[17] in order to reduce Γ. However, due to the electron-surface interaction, there is a lower limit in the Γ value, therefore setting a cap for the maximum σ_{ext}. Thus, extremely high absorption and scattering values seem hardly achievable in practice due to thermal and geometrical limitations.

Finally, by analyzing absorption and scattering under the temperature dependent model, we observe that for high damping conditions and lower aspect ratio structures (e.g., R = 50 nm), scattering and absorption values become comparable, in contrast with the general plasmonic behavior of metallic plasmonic structures, which sees scattering as the main process for large particles[45] (Figure 3c,d).

Figure 5 shows the dependence of the absorption efficiency on the damping Γ, the former calculated at the resonant wavelengths λ_{res}, for golden rods with radius from 10 to 50 nm

dx.doi.org/10.1021/ph500326c | ACS Photonics 2015, 2, 115−120

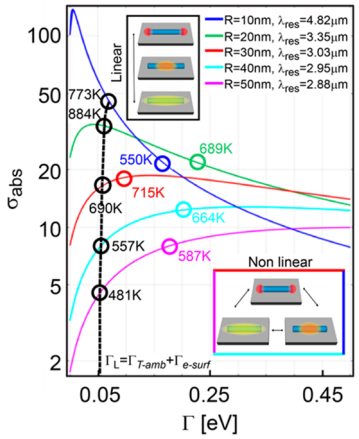

Figure 5. Absorption efficiency of isolated nanorods in air, calculated at the near field resonant wavelengths, versus the damping coefficient Γ. The nanorods have height equal to 1 μm and different radii (log scale). The circles display the steady-state temperature of the structures when interacting with an EM wave of power P = 100 μW and beam waist w_0 = 1 μm. The black circles are associated with the linear (L) model, namely, $\Gamma_L = \Gamma_{T\text{-amb}} + \Gamma_{e\text{-surf}}$. Color circles show the steady-state temperature when the nonlinear (NL) model is utilized, that is, $\Gamma_L = \Gamma_{NL}(T) + \Gamma_{e\text{-surf}}$. The slight bending of the dashed curve is associated with the change in the $\Gamma_{e\text{-surf}}$ due to the geometry variation (the smaller the rods radius, the higher $\Gamma_{e\text{-surf}}$).

(the choice of a Γ independent λ_{res} is supported by Figure 3). The dashed line represents the linear calculation performed at $\Gamma_L = \Gamma_{T\text{-amb}} + \Gamma_{e\text{-surf}}$ for different rod radii, while the continuous lines represent the corresponding non linear case. The slight bending of the dashed line results from the dependence of the damping term $\Gamma_{e\text{-surf}}$ on the rods radius. The black/color circles describe the steady-state temperature reached by the system either under L/NL calculation when a 100 μW power beam with 1 μm waist is considered. By focusing on the NL case, for a 10 nm radius we observe, in most of the Γ range, a rather steep decrease of absorption while the damping (i.e., temperature) increases: the more the structure heats up and its temperature increases, the less the nanorods are likely to dissipate photons into heat. This explains why the NL steady-state temperature (550 K) is lower than the prediction from the linear calculation (773 K, with about 220 K difference): in a L calculation the damping value is fixed ($\Gamma_L = \Gamma_{T\text{-amb}} + \Gamma_{e\text{-surf}}$) and intersects the absorption curves at higher values than the NL case implying a higher capability of converting EM energy into heat (~47 instead of ~21). On the other hand, by unlocking the damping temperature dependence, the solution converges toward a lower value compared to the linear calculations.

By moving to the 50 nm radius configuration we can observe a reverse situation. In fact, being the slope positive in the NL calculation, higher absorption efficiency pushes the final temperature at a higher value with respect to the L case (T_{NL} = 587 K, T_L = 481 K). From these results we can conclude that, both for the L and the NL case, there is no monotone relation between the temperature change and the aspect ratio of the metallic rods.

Figure 5 also confirms the σ_{abs} maps of Figure 3a,c. In fact, it clearly shows that for a 10 nm radius rod, the absorption efficiency tends to decrease for larger Γ, whereas for the 50 nm radius rod it has an opposite behavior.

As previously seen and reported in ref 15, the maxima in the absorption σ_{abs} shown in Figure 3 correspond to the maximization of the dissipated power $P = \mathbf{J} \times \mathbf{E}$. By expressing this expression as $P = \mathrm{Re}(\sigma)|\mathbf{E}|^2$, we can establish general rules of thumb for its optimization. In fact, while the electric field |**E**| resonant wavelength is set by the geometry and is weakly influenced by Γ, the real part of electric conductivity σ presents a maximum when Γ is equal to the frequency ω of the incoming radiation.[25] As a consequence, a number of aspect ratios showing a rather small difference in the absorption efficiency values between the L and NL models can be easily found. For example, in Figure 5 we see how the red curve related to R = 30 nm (λ_{res} = 3.03 μm) exhibits almost the same absorption efficiency and thus the same final temperature both for the L and NL models.

Finally, in order to enhance the difference between the L and NL models, Figure 6 compares the σ_{abs} and σ_{scatt} obtained from

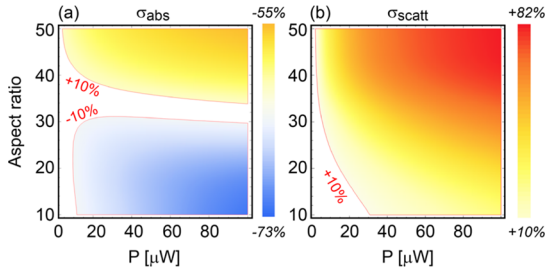

Figure 6. Error committed in calculating σ_{abs} (a) and σ_{scatt} (b) by the linear calculation with respect to the NL model when both the input power and the aspect ratio of the golden nanorods are varied. The nanorods have height h = 1 μm and radius varying from 10 to 50 nm. The calculations are performed at the near field resonant wavelengths. The Gaussian source has a beam waist w_0 = 1 μm. White regions correspond to combination of aspect ratio and input power for which the absolute error of the linear calculation is less than 10%.

the two models by varying the input power and the rods aspect ratio equal to $h/2R$. The plots are calculated in terms of relative difference between the linear and the nonlinear calculation, defined as linear calculation error. Clearly, Figure 6a,b shows quite a different behavior which results from the different dependence of σ_{abs} and σ_{scatt} on the temperature. By considering ±10% as acceptable error value, it is evident that a linear calculation predicts fair values of both absorption and scattering *only* for low input power (P < 10 μW) and low aspect ratio (<30). This important result should be taken into account any time high input power is considered.

To conclude, we have presented temperature dependent electromagnetic calculations on isolated gold nanorods showing the effect of high temperature/intensity incident fields on the optical response of the rods. In general, strong differences are observed between the results from the temperature dependent model and the standard temperature independent model. In particular, striking differences between the two models in absorption efficiency, scattering efficiency and near field enhancement rise by increasing the input power/rods aspect ratio. The presented results are of crucial importance especially when metallic nanodevices, such as sensors, are employed in high temperature environments or when interacting with high intensity electromagnetic sources.

AUTHOR INFORMATION

Corresponding Author

*E-mail: alessandro.alabastri@iit.it.

Notes

The authors declare no competing financial interest.

REFERENCES

(1) Kalousek, R.; Dub, P.; Brínek, L.; Sikola, T. Response of plasmonic resonant nanorods: an analytical approach to optical antennas. *Opt. Express* **2012**, *20*, 17916−17927.

(2) Link, S.; El-Sayed, M. A. Spectral properties and relaxation dynamics of surface plasmon electronic oscillations in gold and silver nanodots and nanorods. *J. Phys. Chem. B* **1999**, *103*, 8410−8426.

(3) Chu, K. C.; Chao, C. Y.; Chen, Y. F.; Wu, Y. C.; Chen, C. C. Electrically controlled surface plasmon resonance frequency of gold nanorods. *Appl. Phys. Lett.* **2006**, *89*, 103107.

(4) De Angelis, F.; Zaccaria, R. P.; Di Fabrizio, E. Mapping the local dielectric response at the nanoscale by means of plasmonic force spectroscopy. *Opt. Express* **2012**, *20*, 29626−29633.

(5) Proietti Zaccaria, R.; De Angelis, F.; Toma, A.; Razzari, L.; Alabastri, A.; Das, G.; Liberale, C.; Di Fabrizio, E. Surface plasmon polariton compression through radially and linearly polarized source. *Opt. Lett.* **2012**, *37*, 545−547.

(6) Proietti Zaccaria, R.; Alabastri, A.; De Angelis, F.; Das, G.; Liberale, C.; Toma, A.; Giugni, A.; Razzari, L.; Malerba, M.; Sun, H. B.; Di Fabrizio, E. Fully analytical description of adiabatic compression in dissipative polaritonic structures. *Phys. Rev. B* **2012**, *86*, 035410.

(7) Alabastri, A.; Toma, A.; Liberale, C.; Chirumamilla, M.; Giugni, A.; De Angelis, F.; Das, G.; Di Fabrizio, E.; Proietti Zaccaria, R. Interplay between electric and magnetic effect in adiabatic polaritonic systems. *Opt. Express* **2013**, *21*, 7538−7548.

(8) De Angelis, F.; Malerba, M.; Patrini, M.; Miele, E.; Das, G.; Toma, A.; Zaccaria, R. P.; Di Fabrizio, E. 3D Hollow Nanostructures As Building Blocks for Multifunctional Plasmonics. *Nano Lett.* **2013**, *13*, 3553−3558.

(9) Panaro, S.; Nazir, A.; Liberale, C.; Das, G.; Wang, H.; De Angelis, F.; Proietti Zaccaria, R.; Di Fabrizio, E.; Toma, A. Dark to bright mode conversion on dipolar nanoantennas: A symmetry-breaking approach. *ACS Photonics* **2014**, *1*, 310−314.

(10) Song, J.; Zaccaria, R. P.; Dong, G.; Di Fabrizio, E.; Yu, M. B.; Lo, G. Q. Evolution of modes in a metal-coated nano-fiber. *Opt. Express* **2011**, *19*, 25206−25221.

(11) Tuccio, S.; Razzari, L.; Alabastri, A.; Toma, A.; Liberale, C.; De Angelis, F.; Candeloro, P.; Das, G.; Giugni, A.; Fabrizio, E. D.; Zaccaria, R. P. Direct determination of the resonance properties of metallic conical nanoantennas. *Opt. Lett.* **2014**, *39*, 571−573.

(12) Bisio, F.; Proietti Zaccaria, R.; Moroni, R.; Maidecchi, G.; Alabastri, A.; Gonella, G.; Giglia, A.; Andolfi, L.; Nannarone, S.; Mattera, L.; Canepa, M. Pushing the high-energy limit of plasmonics. *ACS Nano* **2014**, *8*, 9239−9247.

(13) Joy, N. A.; Janiszewski, B. K.; Novak, S.; Johnson, T. W.; Oh, S.-H.; Raghunathan, A.; Hartley, J.; Carpenter, M. A. Thermal stability of gold nanorods for high-temperature plasmonic sensing. *J. Phys. Chem. C* **2013**, *117*, 11718−11724.

(14) Yeshchenko, O. A.; Bondarchuk, I. S.; Gurin, V. S.; Dmitruk, I. M.; Kotko, A. V. Temperature dependence of the surface plasmon resonance in gold nanoparticles. *Surf. Sci.* **2013**, *608*, 275−281.

(15) Nepal, D.; Park, K.; Vaia, R. A. Gold nanorods: High-yield assembly of soluble and stable gold nanorod pairs for high-temperature plasmonics. *Small* **2012**, *8*, 1013−1020.

(16) Albella, P.; Alcaraz de la Osa, R.; Moreno, F.; Maier, S. A. Electric and magnetic field enhancement with ultralow heat radiation dielectric nanoantennas: considerations for surface-enhanced spectroscopies. *ACS Photonics* **2014**, *1*, 524−529.

(17) Bouillard, J.-S. G.; Dickson, W.; O'Connor, D. P.; Wurtz, G. A.; Zayats, A. V. Low-temperature plasmonics of metallic nanostructures. *Nano Lett.* **2012**, *12*, 1561−1565.

(18) Baffou, G.; Girard, C.; Quidant, R. Mapping heat origin in plasmonic structures. *Phys. Rev. Lett.* **2010**, *104*, 136805.

(19) Link, S.; El-Sayed, M. A. Size and temperature dependence of the plasmon absorption of colloidal gold nanoparticles. *J. Phys. Chem. B* **1999**, *103*, 4212−4217.

(20) Chiang, H. P.; Chen, C. W.; Wu, J. J.; Li, H. L.; Lin, T. Y.; Sánchez, E. J.; Leung, P. T. Effects of temperature on the surface plasmon resonance at a metal−semiconductor interface. *Thin Solid Films* **2007**, *515*, 6953−6961.

(21) Lereu, A. L.; Passian, A.; Farahi, R. H.; van Hulst, N. F.; Ferrell, T. L.; Thundat, T. Thermoplasmonic shift and dispersion in thin metal films. *J. Vac. Sci. Technol., A* **2008**, *26*, 836−841.

(22) Daneshfar, N. Temperature dependence of the optical characteristics and surface plasmon resonance of core-shell nanoparticles. *Phys. Plasmas* **2014**, *21*, 063301.

(23) Govorov, A. O.; Richardson, H. H. Generating heat with metal nanoparticles. *Nano Today* **2007**, *2*, 30−38.

(24) Baffou, G.; Quidant, R. Thermo-plasmonics: using metallic nanostructures as nano-sources of heat. *Laser Photonics Rev.* **2013**, *7*, 171−187.

(25) Alabastri, A.; Tuccio, S.; Giugni, A.; Toma, A.; Liberale, C.; Das, G.; De Angelis, F.; Di Fabrizio, E.; Proietti Zaccaria, R. Molding of plasmonic resonances in metallic nanostructures: Dependence of the nonlinear electric permittivity on system size and temperature. *Materials* **2013**, *6*, 4879−4910.

(26) Hou, W.; Cronin, S. B. A review of surface plasmon resonance-enhanced photocatalysis. *Adv. Funct. Mater.* **2013**, *23*, 1612−1619.

(27) Honda, M.; Kumamoto, Y.; Taguchi, A.; Saito, Y.; Kawata, S. Plasmon-enhanced UV photocatalysis. *Appl. Phys. Lett.* **2014**, *104*, 061108.

(28) Schwede, J. W.; Bargatin, I.; Riley, D. C.; Hardin, B. E.; Rosenthal, S. J.; Sun, Y.; Schmitt, F.; Pianetta, P.; Howe, R. T.; Shen, Z.-X.; Melosh, N. A. Photon-enhanced thermionic emission for solar concentrator systems. *Nat. Mater.* **2010**, *9*, 762−767.

(29) Guler, U.; Boltasseva, A.; Shalaev, V. M. Refractory plasmonics. *Science* **2014**, *344*, 263−264.

(30) Guler, U.; Ndukaife, J. C.; Naik, G. V.; Nnanna, A. G. A.; Kildishev, A. V.; Shalaev, V. M.; Boltasseva, A. Local heating with lithographically fabricated plasmonic titanium nitride nanoparticles. *Nano Lett.* **2013**, *13*, 6078−6083.

(31) Liu, J.; Guler, U.; Li, W.; Kildishev, A.; Boltasseva, A.; Shalaev, V. M. High-temperature plasmonic thermal emitter for thermo-photovotaics. CLEO: 2014, San Jose, California, 2014/06/08; Optical Society of America: San Jose, CA, 2014; p FM4C.5.

(32) Rakic, A. D.; Djurisic, A. B.; Elazar, J. M.; Majewski, M. L. Optical properties of metallic films for vertical-cavity optoelectronic devices. *Appl. Opt.* **1998**, *37*, 5271−5283.

(33) Gurzhi, R. N. *J. Exp. Theor. Phys.* **1958**, *6*, 506.

(34) Lawrence, W. E. Electron-electron scattering in the low-temperature resistivity of the noble metals. *Phys. Rev. B* **1976**, *13*, 5316−5319.

(35) Holstein, T. Theory of transport phenomena in an electron-phonon gas. *Ann. Phys.* **1964**, *29*, 410−535.

(36) Gurzhi, R. N.; Kaganov, M. I. Effect of Interelectron Collisions on the Optical Properties of Metals. *J. Exp. Theor. Phys.* **1966**, *22*, 654−656.

(37) Gurzhi, R. N.; Azbel, M. Y.; Lin, X. B. Surface effects in infrared optics. *Phys. Solid State* **1963**, *5*, 554−559.

(38) Lawrence, W. E.; Wilkins, J. W. Electron−electron scattering in the transport coefficients of simple metals. *Phys. Rev. B* **1973**, *7*, 2317−2332.

(39) Holstein, T. Optical and infrared volume absorptivity of metals. *Phys. Rev.* **1954**, *96*, 535−536.

(40) Biondi, M. A.; Rayne, J. A. Band structure of noble metal alloys: Optical absorption in α-brasses at 4.2 K. *Phys. Rev.* **1959**, *115*, 1522−1530.

(41) McKay, J. A.; Rayne, J. A. Temperature dependence of the infrared absorptivity of the noble metals. *Phys. Rev. B* **1976**, *13*, 673−685.

(42) Coronado, E. A.; Schatz, G. C. Surface plasmon broadening for arbitrary shape nanoparticles: A geometrical probability approach. *J. Chem. Phys.* **2003**, *119*, 3926−3934.

(43) Piatkowski, L.; Hugall, J. T.; van Hulst, N. F. Raman spectroscopy: Watching a molecule breathe. *Nat. Photonics* **2014**, *8*, 589−591.
(44) Atwater, H. A.; Polman, A. Plasmonics for improved photovoltaic devices. *Nat. Mater.* **2010**, *9*, 205−213.
(45) Hecht, L. N. a. B. *Principles of Nano-Optics*; Cambridge University Press: New York, NY, U.S.A., 2006.